1994ApJ...420..183S

THE ASTROPHYSICAL JOURNAL, 420:183–196, 1994 January 1
© 1994. The American Astronomical Society. All rights reserved. Printed in U.S.A.

HIGHLY IONIZED GAS ABSORPTION IN THE DISK AND HALO TOWARD HD 167756 AT 3.5 KILOMETERS PER SECOND RESOLUTION[1]

BLAIR D. SAVAGE
Washburn Observatory, University of Wisconsin, 475 North Charter Street, Madison, WI 53706
KENNETH R. SEMBACH
Center for Space Research, Building 37, MIT, Cambridge, MA 02139
AND
JASON A. CARDELLI
Washburn Observatory, University of Wisconsin, 475 North Charter Street, Madison, WI 53706
Received 1993 April 19; accepted 1993 July 13

ABSTRACT

High-resolution spectra of interstellar Si IV, C IV, and N V absorption lines along the 4 kpc path to the inner Galaxy star HD 167756 at $z = -0.85$ kpc are presented. The spectra were obtained with the echelle mode of Goddard High Resolution Spectrograph (GHRS) aboard the *Hubble Space Telescope* (*HST*) and have signal-to-noise ratios ranging from 23 to 38. The high resolution of the measurements (FWHM = 3.5 km s^{-1}) results in fully resolved line profiles for the highly ionized gas absorption. The measurements provide information on the column density per unit velocity, $N(v)$, as a function of velocity for Si IV, C IV, and N V. The C IV and N V profiles extend from -70 to $+70$ km s^{-1}, while the Si IV profiles extend from -40 to $+70$ km s^{-1}. The integrated logarithmic column densities are long N(Si IV) = 13.09 ± 0.02, log N(C IV) = 13.83 ± 0.02, and log N(N V) = 13.56 ± 0.03. The N V profile is broad, asymmetric, and featureless, while the Si IV profile contains narrow absorption components near $v_{LSR} = -19$, 0, $+20$, and $+52$ km s^{-1} with Doppler spread parameters, $b \approx 10$–12 km s^{-1}. The C IV profile contains both broad and narrow structure. The high ion feature near $+52$ km s^{-1} is also detected in the low-ionization lines of Ca II, O I, Si II, and Fe II. The other narrow Si IV and C IV components occur within several km s^{-1} of components seen in low-ionization species. The sight line contains at least two types of highly ionized gas. One type gives rise to a broad N V profile, and the other results in the more structured Si IV profile. The C IV profile contains contributions from both types of highly ionized gas. The broad but asymmetric N V profile is well represented by a large Galactic scale height gas which is participating in Galactic rotation and has a combination of thermal and turbulent broadening with $b_{tot} \approx 42$ km s^{-1}. The C IV to N V abundance ratio of 1.0 ± 0.3 for the gas implies $T \sim 1.6 \times 10^5$ K or $\sim 8 \times 10^5$ K if the gas is in collisional ionization equilibrium and has a solar carbon to nitrogen abundance ratio. This absorption may be associated with cooling hot gas situated in Galactic shells and supershells along the sight line. The gas producing the narrow Si IV and C IV absorption components has line widths that are compatible with origins in conductive interfaces between the warm and hot interstellar medium. Kinematic flows associated with the photoionized edges of clouds might also produce Si IV and C IV lines with Doppler spread parameters similar to those observed, but the C IV to Si IV ratio in this gas is 3.5, which leads us to favor the conductive interface interpretation.

Subject headings: Galaxy: halo — ISM: abundances — stars: individual (HD 167756) — ultraviolet: interstellar

1. INTRODUCTION

We present high spectral resolution UV observations of Si IV, C IV, and N V absorption along the sight line to the distant halo star HD 167756. The observations were obtained to study the ionization processes occurring in the warm and hot phases of the interstellar medium in the Galactic disk and low halo. The star is located in the direction $l = 351.^\circ5$ and $b = -12.^\circ3$ about 4 kpc from the Sun at a Galactic altitude $z = -0.85$ kpc. We obtained the photon-counting UV spectra with the Goddard High Resolution Spectrograph (GHRS) operating in the echelle mode. A separate paper will contain a study of GHRS observations of neutral gas toward HD 167756 (Cardelli, Sembach, & Savage 1993, hereafter Paper II). The high resolution of the GHRS echelle model data (FWHM ~ 3.5 km s^{-1}) permits a direct study of profile similarities and differences for three important tracers of the highly ionized medium between the stars.

The organization of this paper is as follows: In § 2 we describe the observations and data handling. An overview of the sight line characteristics is presented in § 3. We present absorption-line velocities, equivalent widths, and column densities for the highly ionized gas in § 4. In § 5 we discuss the origin of the highly ionized gas toward HD 167756. We summarize our results in § 6.

2. OBSERVATIONS AND REDUCTION

GHRS echelle observations of various interstellar lines in the spectrum of HD 167756 were obtained in 1991 June, several weeks before the low-voltage power supply on Side 1 of

[1] Based on observations with the NASA/ESA *Hubble Space Telescope*, obtained at the Space Telescope Science Institute which is operated by the Association of Universities for Research in Astronomy, Inc., under NASA contract NAS5-26555.

© American Astronomical Society • Provided by the NASA Astrophysics Data System

1994ApJ...420..183S

the GHRS malfunctioned. The observations were obtained with the light of HD 167756 positioned in the small (0".25 × 0".25) entrance aperture to preserve the full spectroscopic resolution of the GHRS (FWHM ~3.5 km s^{-1}). Digicon detector scanning (step-pattern number 6) was used to provide two spectrum samples per diode width and measurements of the interorder background with the full array of 500 diodes. Four diode comb-addition and the FP-SPLIT = 6 procedure were used for each set of exposures. Comb-addition averages the detected spectrum over four Digicon detector diodes. The FP-SPLIT sequence breaks each spectral integration into four subexposures, each shifted by five diodes from the previous subexposure by a grating rotation. By aligning and combining the individual FP-SPLIT subexposures, the photocathode and detector window fixed pattern noise were reduced. On-Board Doppler compensation was enabled to correct for spacecraft motion during all observations. Details regarding the GHRS and its Digicon detectors are given by Duncan & Ebbets (1989). GHRS inflight performance results are discussed by Ebbets (1992).

The exposure log for the HD 167756 GHRS data is given in Table 1. The entries include the spectrum identification number, the echelle order number, the spectral range covered in each 500 diode Digicon spectrum, the spectral resolution (FWHM) in km s^{-1}, the exposure time in seconds, a scattered light correction parameter, the spectral merging method, the spectral calibration velocity offset correction, and the detected interstellar species.

We followed the data reduction procedure of Savage, Cardelli, & Sofia (1992) for data extraction, background processing and subtraction, and wavelength calibration of the data. The calibration files and procedures used are equivalent to those implemented in the Space Telescope Science Institute's Routine Science Data Processing (RSDP) files as of 1992 June. These files are preserved in the *HST* data archive. For all lines, we applied a residual scattered light correction according to the prescription outlined by Cardelli, Ebbets, & Savage (1990, 1993). The value of the constant d used in the correction is given in Table 1. Constant c was taken to be 0.00.

Echelle mode exposures obtained when the maximum absolute value of the orbital Doppler correction is required may contain an error in that correction. The error may result in FP-SPLIT subexposures with invalid velocity shifts or artificially broadened profiles. Subexposures in four of our observations were identified as being suspected of having shifts up to 2.75 diodes (see Table 1). The high ion lines are broad compared to the expected shifts, and our integrations were broken into many (12–24) subexposures to reduce the effects of problems that any individual subexposures may suffer. We checked the individual high ion FP-SPLIT subexposures and found that within the observational errors, the high ion lines do not suffer from a significant loss of resolution or have large velocity shifts.

We merged the individual FP-SPLIT measurements using either the standard merge or centroid merge algorithms as indicated in Table 1. The standard merge algorithm used the nominally assigned wavelengths as the alignment reference, while centroid merge aligns the subexposures with respect to the derived centroids of observed spectral features. Centroid merge produces a better alignment provided the spectrum contains narrow spectral features that are well observed.

The combined data have a resolution of approximately 3.5 km s^{-1} (FWHM) and signal-to-noise ratios of 23 to 38 per diode subset. The S/N is a factor of 1.5 to 2 lower than expected because the light of HD 167756 was not optimally centered in the GHRS small entrance aperture.

To bring the interstellar absorption lines into a common velocity system, we employed a velocity "bootstrap" adjustment method similar to the one used for the ξ Per measurements by Cardelli et al. (1991). The Mg II $\lambda\lambda$1239, 1240 lines were used to tie the N V $\lambda\lambda$1238, 1242 observations into the velocity frame of the neutral gas tracers. The discrete absorption feature at +52 km s^{-1} (LSR) seen in both low and high ionization lines was used to tie the Si IV λ1393 and C IV $\lambda\lambda$1548, 1550 lines into the same system. An additional velocity shift was applied to bring the bootstrapped velocity system into the heliocentric velocity frame found for Na I and Ca II ground-based observations for HD 167756 (Sembach, Danks, &

TABLE 1

OBSERVATIONS[a]

Observation[b] ID	Echelle Order	Wavelength Coverage (Å)	FWHM[c] (km s^{-1})	Exposure Time[d] (s)	Scattered Light Correction[e]	Merge Type[f]	Velocity Shift[g] (km s^{-1})	Species Detected
Z0JA010BM*	A36	1549.98–1553.29	3.60	921.6	0.04	S	−5.6	C IV
Z0JA010EM*	A40	1388.24–1395.76	3.53	896.0	0.04	S	−3.5	Si IV
Z0JA010IM*	A43	1298.17–1305.05	3.53	358.4	0.05	C	+0.9	O I, P II, Si II
Z0JA010LM*	A45	1237.76–1244.38	3.62	614.4	0.05	C	+2.2	N V, Mg II
Z0JA010RT	B31	1801.30–1810.95	3.53	307.2	0.04	C	−1.7	Si II, S I

[a] All observations were obtained with the light of the star in the small (0".25 × 0".25) science aperture (SSA). All exposures employed Digicon scanning step-pattern 6 at a sampling interval of two substeps per diode width using either Ech-A or ECh-B and the FP-SPLIT technique to reduce fixed-pattern noise.

[b] *HST* archive identification. Entries marked with an asterisk may contain individual spectral integrations that are affected by an error in the Doppler compensation correction. We checked the individual FP-SPLIT exposures for these observations and found no noticeable degradation in the resolution of the composite spectrum as a result of individual FP-SPLIT subexposures suffering from the Doppler compensation problem discussed in the text (see § 2).

[c] Instrumental resolution (FWHM) in km s^{-1}.

[d] Total on-spectrum exposure time.

[e] Scattered light "d" correction (see text).

[f] Type of merging used to combine individual FP-split observations: C = centroid merge, S = standard merge (see text).

[g] Velocity shift required to bring the spectra into the heliocentric velocity reference frame. For C IV and Si IV the shift assumes that the narrow component detected near 52 km s^{-1} occurs at the same velocity as lower ionization features. An additional shift of +5.5 km s^{-1} is required to bring the heliocentric veocities into the local standard of rest velocity reference frame.

© American Astronomical Society • Provided by the NASA Astrophysics Data System

1994ApJ...420..183S

Savage 1993). The ± 52 km s^{-1} feature seen in O I λ1302, Si II λ1304, and Ca II λ3933 served as a reference between the GHRS and ground based data. The velocity shift applied to each observation to bring it into the heliocentric frame is listed in Table 1. The two largest shifts are for C IV (-5.6 km s^{-1}) and Si IV (-3.5 km s^{-1}). These shifts are twice as large as the velocity shifts typically found for GHRS echelle observations (see Savage et al. 1992). The magnitude of the shifts depends on the assumption that the 52 km s^{-1} feature actually occurs at that velocity. If this feature involves some type of dynamical phenomenon such as a shock, there may be a small additional velocity offset between the low and high ion lines. A final shift of $+5.5$ km s^{-1} was applied to all heliocentric velocities to bring them into the local standard of rest using the assumption of a solar neighborhood speed of $+16.5$ km s^{-1} in the direction $l = 53°, b = 25°$ (Mihalas & Binney 1981).

3. THE HD 167756 SIGHT LINE

HD 167756 lies in the inner Galaxy in the direction $l = 351.°5$, $b = -12.°3$. It was classified B0.5 Ia by Garrison, Hiltner, & Schild (1969, 1977) on the basis of high-dispersion optical spectra. We have verified the optical classification by examining the ultraviolet spectrum of the star (see Appendix A in Paper II). Using the observed colors of the star ($V = 6.30$, $B-V = -0.13$; Schild, Garrison, & Hiltner 1983) and the intrinsic colors given by Johnson (1963), we derive a color excess $E(B-V) = 0.09$. We calculate the spectroscopic distance $d = 4.0$ kpc assuming the Population I absolute magnitude system derived by Walborn (1972) and the relation $A_V = 3.1E(B-V)$. At the distance, the star lies at the Galactic altitude $z = -0.85$ kpc and a galactocentric distance $R = 4.7$ kpc assuming $R_0 = 8.5$ kpc.

With a hydrogen column density $N(\text{H I}) = 6.5 \times 10^{20}$ atoms cm^{-2} based on an analysis of the Lyman-α line (Diplas & Savage 1993), the average sight line density of neutral hydrogen is $\langle n_{\text{H I}} \rangle = 0.053$ atoms cm,$^{-3}$. Much of the sight line evidently passes through relatively low density phases of the interstellar medium (see Paper II).

H I 21 cm emission line data shown by Danly et al. (1992) for the HD 167756 direction reveal that the H I emission profile has maximum brightness at $+5.5$ km s^{-1} and a broad weak component centered near $+30$ km s^{-1}. Weak wings of 21 cm emission can be seen to -105 and to $+80$ km s^{-1}. Some of this high velocity emission must be coming from beyond the star. The total H I column density determined from the 21 cm emission data, assuming $T_{\text{spin}} = 75$ K, is 9.5×10^{20} atoms cm^{-2} (Danly et al. 1992). A comparison of this column density with the value from Lyman-α absorption suggests that the H I column density beyond the star is approximately 3×10^{20} atoms cm^{-2} or about one-third of the total H I in this direction.

Measurements of Ca II and Na I toward HD 167756 at a resolution of 5 km s^{-1} are presented by Sembach et al. (1993). The spectra reveal a complex multicomponent neutral absorbing medium with eight components identified in the Ca II absorption over the LSR velocity range from -36 to $+52$ km s^{-1} (see Figs. 1 and 2). The strongest component occurs at $+6.5$ km s^{-1}. Table 2 lists the absorption lines shown in Figures 1 and 2.

Approximately one-third of the sight line to HD 167756 is confined to the Galactic plane ($|z| < 250$ pc). The sight line passes through the local interstellar medium as well as the more general environment of the Galactic disk and low halo. Galactic rotation effects are relatively small over the 4 kpc path length to the star. The radial velocity of gas participating in Galactic rotation decreases approximately linearly from 0 km s^{-1} to -26 km s^{-1} over the 4 kpc path to HD 167756, assuming a galactocentric distance of 8.5 kpc, a circular rotation speed of 220 km s^{-1} for the solar neighborhood, and the Galactic rotation curve of Clemens (1985). The observed LSR radial velocity of HD 167756 is -20 km s^{-1} (Wilson 1953).

The HD 167756 sight line passes under several spiral arms. The Sagittarius spiral arm is located between 1 and 2 kpc from the Sun and extends from $l = 330°$ to 30° (Courtes, Georgelin, & Monnet 1970; Georgelin & Georgelin 1976). Courtès et al. find H II region velocities of ≈ -10 km s^{-1} associated with the Sagittarius arm at $l = 350°$. Rickard (1974) finds peculiar velocities on the order of 40 km s^{-1} associated with the arm between $l = 340°$ and 0°, beginning at about 1 kpc. Assuming a distance of 1.5 kpc for the arm, the HD 167756 sight line passes under the arm at $z = -0.32$ kpc. Corotating gas would have a radial velocity of -8 km s^{-1} at this distance. Georgelin & Georgelin (1976) define another independent spiral arm in this direction based upon a survey of H109α emission and optical H II regions and OB associations. The estimated distance to the Scutum-Crux arm is 3 kpc. At this distance corotating gas would have a radial velocity of -17 km s^{-1} and the sight line would pass under the arm at $z = -0.64$ kpc. It is unlikely that the HD 167756 sight line will be influenced by the Norma Spiral arm extending from $l = 305°$ to 333° (Courtès et al.

TABLE 2

ABSORPTION LINES SHOWN IN FIGURES 1 AND 2

Ion	IP(x^{i-1})[a] (eV)	IP(x^{i})[a] (eV)	Wavelength[b] (Å)	f-value[b]	Component
Ca II	6.11	11.87	3933.663	0.6346	From Sembach, Danks, & Savage 1993
Si II	8.15	16.34	1808.013	0.0055	S I λ1807.31 located at -116 km s^{-1}
	8.15	16.34	1304.370	0.1473	
Si IV	33.49	45.14	1393.755	0.5140	
C IV	47.89	64.49	1550.770	0.0952	
	47.49	64.49	1548.195	0.1908	
N V	77.47	97.89	1242.804	0.0782	Uncertain continuum
	77.47	97.89	1238.821	0.1570	

[a] Ionization potential (eV) required to create and destroy ion from Moore 1970.
[b] Rest wavelengths and f-values from Morton 1991. The Ca II wavelength is for air; the others are for vacuum.

© American Astronomical Society • Provided by the NASA Astrophysics Data System

1994ApJ...420..183S

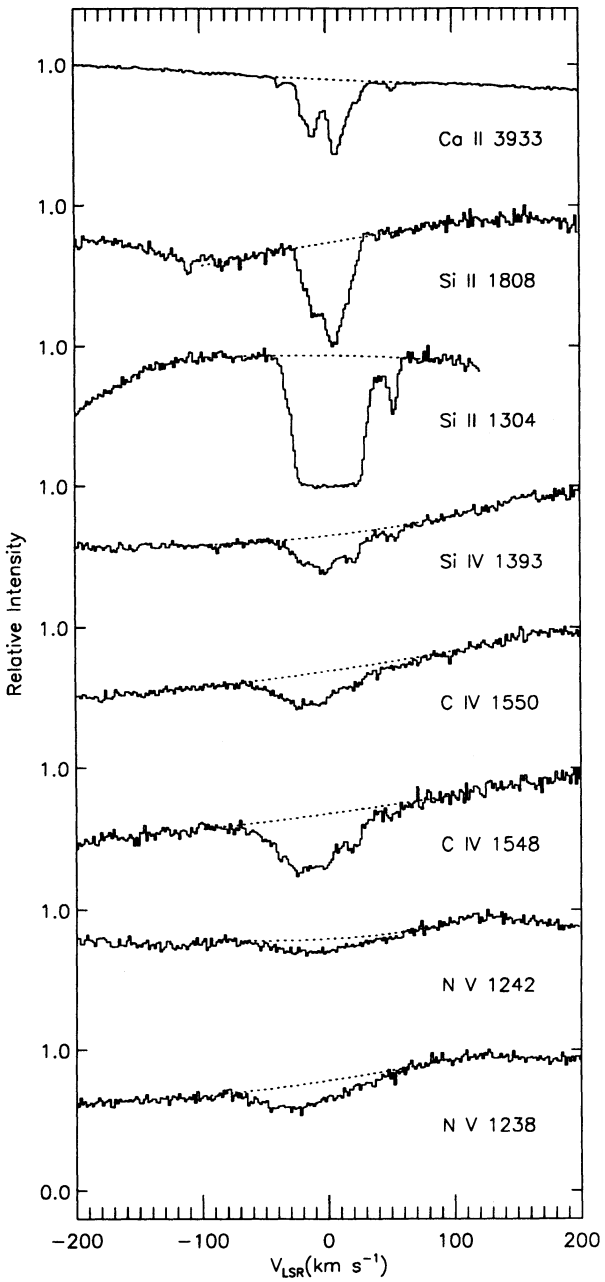

FIG. 1.—Observed absorption-line profiles for the indicated species as a function of LSR velocity (km s^{-1}). Table 2 provides atomic parameters for the absorption lines illustrated. The zero level for each profile coincides with the 1.0 level of the next lower profile. The high-ionization absorption lines of C IV and N V occur on the relatively smooth stellar P Cygni profiles of these same species. For each absorption line the continuum level used to produce the continuum normalized line profiles of Fig. 2 is shown with the dashed line. For the Si II λ1808, line, a weak absorption of S I λ1807.31 appears at $v = -116$ km s^{-1}. The measurements for Ca II λ3933 are from Sembach, Danks, & Savage (1993).

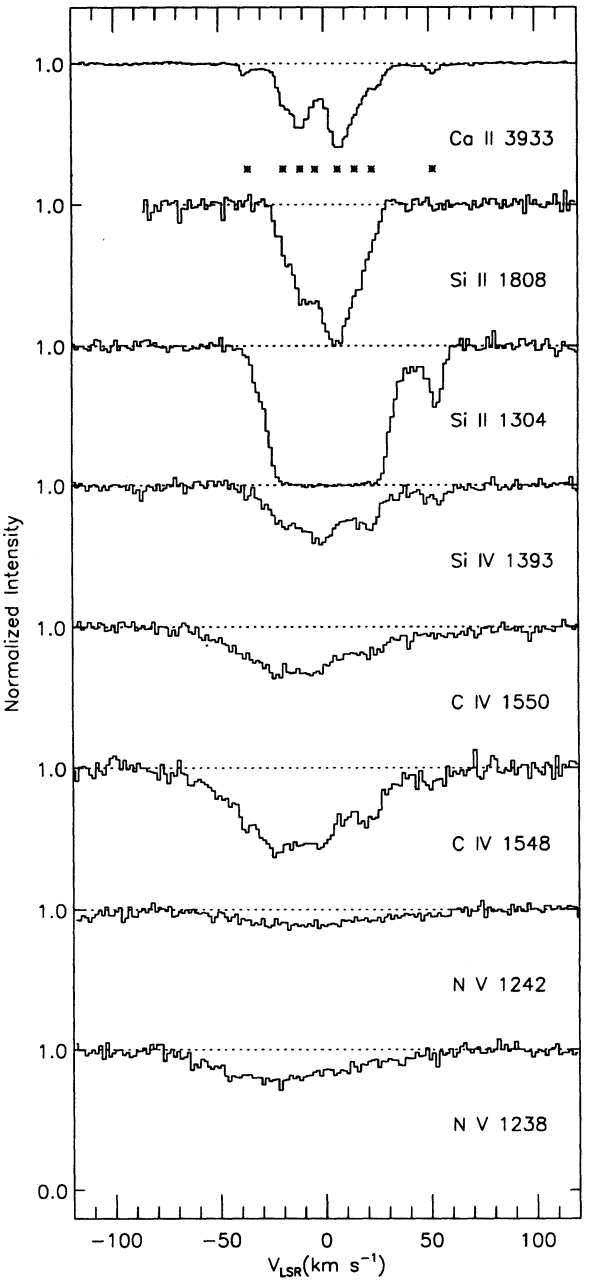

FIG. 2.—Continuum-normalized absorption-line profiles for the data illustrated in Fig. 1 are plotted against LSR velocity (km s^{-1}). The zero level for each profile coincides with the 1.0 level of the next lower profile. The asterisks below the Ca II profile indicate the velocities of absorption components detected in Ca II. Note the component structure in the lines of Si IV and C IV that is not apparent in the N V absorption. The isolated component near +52 km s^{-1} seen in Si IV and C IV is also apparent in the absorption of Ca II λ3933 and Si II λ1304.

1970; Georgelin & Georgelin 1976) or by the 3 kpc expanding arm (Oort 1970) in the inner Galaxy.

The HD 167756 sight line passes under a number of structures that may relate to the venting of gas into the Galactic halo. Koo, Heiles, & Reach (1992) have identified Galactic "worm" structures detected in H I 21 cm and infrared emission that are believed to be the walls surrounding superbubbles that have broken through the thin disk gas. Several of these structures extend outward from the Galactic disk from $l = 345°$ to 355°. The 21 cm emission maps shown in Figure 13 of Koo et al. (1992) reveal the possible presence of two superbubbles in the velocity range from -20 to -28 km s^{-1} which seem to be associated with Galactic worms GW 344.9−2.8, GW 346.5−7.0, GW 350.7−3.5, and GW 354.3−5.3. The bubbles are centered at $l = 347°$, $b = -5°$ and $l = 352°$, $b = -3°$ and appear to open into the halo.

The UV absorption line spectrum of HD 167756 has been studied using data from the *International Ultraviolet Explorer*

© American Astronomical Society • Provided by the NASA Astrophysics Data System

1994ApJ...420..183S

(*IUE*) *Satellite* (Savage & Massa 1987; Danly et al. 1992; Sembach & Savage 1992). The highest quality data are those of Sembach & Savage (1992) who combined seven *IUE* spectra to study the highly ionized gas toward HD 167756 at a resolution of 25 km s^{-1}. The *IUE* results indicate the HD 167756 sight line has a lower than average ratio of C IV to N V (1.6 vs. 4.6 ± 2.7) and a slightly higher ratio of C IV to Si IV than average (4.8 vs. 3.6 ± 1.3). These differences appear to be due to a combination of slight enhancement in the amount of N V ($\sim$1.6x) and a deficiency in the amount of Si IV and C IV ($\sim$2.1x to 3.7x) compared to the average disk/halo sight line observed in the survey of Sembach & Savage (1992). We compare their measurements to the GHRS results in § 4.4.

4. Si IV, C IV, AND N V ABSORPTION

The high ion lines of Si IV λ1393, C IV $\lambda\lambda$1548, 1550, and N V $\lambda\lambda$1238, 1242 are shown in the bottom portion of Figure 1 where the observed intensity is plotted against LSR velocity. The C IV lines are superposed on the gently sloping continuum of a well-developed stellar P Cygni profile. The N V lines also lie on a P Cygni profile. We detected a small change in the profile longward of 1240 Å between the time the echelle observations and subsequent first-order observations of lower resolution were obtained. We see no such change in the C IV P Cygni profile during the same time frame. The Si IV λ1393 line lies on the stellar profile at a location of moderate continuum curvature. The dashed lines in Figure 1 show our estimates of the continuum level for each absorption line. These continua were used to produce the continuum normalized line profiles for each feature shown in Figure 2. The continuum placement for the N V λ1242 line is uncertain. Weak absorption of unknown but likely stellar origin exists over the velocity range from approximately -100 to -180 km s^{-1}. That absorption is not due to interstellar N V since it does not appear in the stronger λ1238 line.

The high ion lines shown in Figure 2 are broad with large negative and positive extensions. The Si IV λ1393 profile extends from -40 km s^{-1} to $+70$ km s^{-1} and has FWHM = 52 km s^{-1}. The C IV λ1548 and N V λ1238 profiles are broader than the Si IV λ1393 profile and extend from -70 km s^{-1} to $+70$ km s^{-1}. The FWHM of the C IV λ1548 and N V λ1238 profiles are 67 and 73 km s^{-1}, respectively. The Si IV and C IV profiles contain narrow absorption features. The most prominent examples are near 0, $+21$, and $+52$ km s^{-1}. The high ion profiles can be compared with the Ca II λ3933 and Si II $\lambda\lambda$1808, 1304 lines shown in Figures 1 and 2. Other examples of low ion absorption profiles can be found in Paper II.

4.1. *Apparent Column Density Profiles and Ionic Ratios*

The very high resolution and quality of the measurements illustrated in Figures 1 and 2 provides an excellent opportunity to study the detailed character of the high ion absorption lines. We represent the data in the form of apparent column density as a function of velocity. An apparent column density profile can be constructed for each absorption line acording to

$$N_a(v)[\text{atoms cm}^{-2}\ (\text{km s}^{-1})^{-1}] = (m_e c/\pi e^2)(f\lambda)^{-1}\tau_a(v) = 3.768 \times 10^{14}(f\lambda)^{-1}\tau_a(v)\,, \quad (1)$$

where f is the oscillator strength of the line, λ is the wavelength of the line in Å, and $\tau_a(v)$ is the apparent optical depth given by

$$\tau_a(c) = \ln[I_c(v)/I(v)]\,, \quad (2)$$

where $I(v)$ is the observed line intensity at velocity v and $I_c(v)$ is the estimated continuum intensity at velocity v. In the limit where the line is resolved by the spectrograph, as is likely the case for the high-ionization lines, $\tau_a(v) \approx \tau(v)$, the true optical depth of the line, and $N_a(v) \approx N(v)$, the true column density per unit velocity.

The data presented here represent one of the few observations of highly ionized interstellar gas at a resolution capable of fully resolving the absorption profiles (also see Spitzer & Fitzpatrick 1992; Sembach, Savage, & Jenkins 1994). Under conditions where recombinations balance collisional ionizations, the temperatures at which Si IV, C IV, and N V peak in abundance are 6.6×10^4, 1.0×10^5 and 1.8×10^5 K, respectively (Sutherland & Dopita 1993). The corresponding thermal line widths (FWHM) for each of the three ions at these temperatures are 10, 20, and 24 km s^{-1}. These widths are 3–4 times larger than the 4–6 km s^{-1} widths expected for these ions in 10^4 K photoionized gas. Both the collisionally ionized and photoionized widths are larger than the 3.5 km s^{-1} (FWHM) of the instrumental spread function of the GHRS. Therefore, the high ion lines should be resolved regardless of whether they are produced by photoionization or collisional ionization.

One can compare the $N_a(v)$ profiles for lines within a species differing in the product $f\lambda$ to determine whether unresolved saturated structure exists within the profiles. In cases where unresolved saturated structure does exist, the $N_a(v)$ profile for the stronger line will underestimate the value of $N_a(v)$ for the weaker line by the significant amount at the velocities of the saturated structure. The ability to discern these profile differences depends upon both the relative strengths of the lines and the quality of the data. A review of the technique has been given by Savage & Sembach (1991). Recent uses of this technique can be found in Joseph & Jenkins (1991) and Sembach & Savage (1992 and references therein).

In Figure 3 we compare the apparent column density profiles for the C IV $\lambda\lambda$1548, 1550 lines. The strong and weak components of each doublet are plotted as solid and dashed

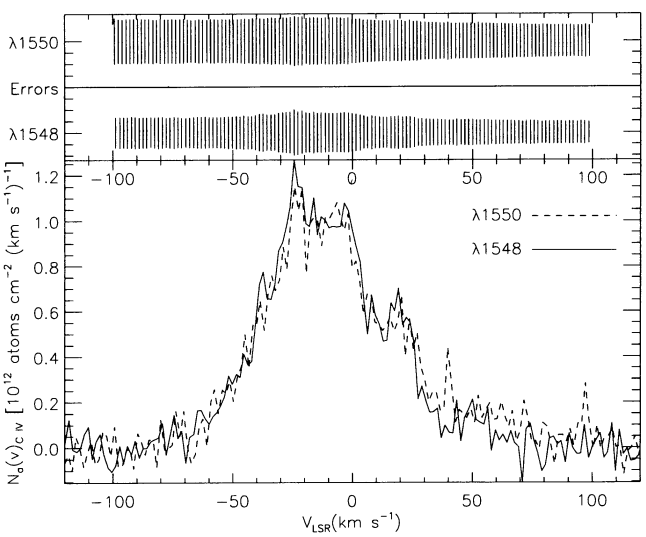

FIG. 3.—Apparent column density, $N_a(v)$ [atoms cm^{-2} (km s^{-1})$^{-1}$], vs. LSR velocity (km s^{-1}) for each component of the C IV doublet. The $N_a(v)$ curves for C IV $\lambda\lambda$1548, 1550 are shown as solid and dashed curves, respectively. The errors ($\pm 1\ \sigma$) produced by continuum placement and statistical uncertainties are illustrated at the top of the figure for each $N_a(v)$ curve. The good agreement between the two $N_a(v)$ curves reveals that the C IV profiles do not contain unresolved saturated structure.

© American Astronomical Society • Provided by the NASA Astrophysics Data System

1994ApJ...420..183S

lines, respectively. The corresponding error bars are plotted above the profiles. Within the errors introduced by continuum placement and statistical uncertainties, the weak and strong components of the C IV apparent column density profiles agree with one another, indicating that these profiles do not contain unresolved saturated structure. The $N_a(v)$ curves derived from the two N V absorption lines (not illustrated here) also agree well. Although only one line of the Si IV doublet was observed, it is equally likely that it does not contain unresolved saturated structure given the high resolution of the spectrograph and the strength of the λ1393 line which is between that for the two C IV lines. Given these considerations, the values of the apparent optical depths for the high ionization absorption lines should provide valid descriptions of the true optical depths after accounting for a minor amount of instrumental smearing due to the finite spectrograph resolution. Since the data quality is higher for the stronger member of each high ion doublet, we concentrate on the $N_a(v)$ curves based on the stronger member of each doublet in the following discussions.

Plots of $N_a(v)$ for Si II, Si IV, C IV, and N V as a function of LSR velocity are shown in Figure 4. The errors represent 1 σ uncertainties due to statistical noise and continuum placement. For Si II the results shown are based on the λ1808 line and the stronger λ1304 line. The weaker line traces the behavior of $N_a(v)$ where it is largest, while the stronger line provides information about small values of $N_a(v)$ at high velocities. The Si II $N_a(v)$ profile is much more strongly peaked near 0 km s^{-1} than the high ion profiles. This is also true for the profiles of Na I, Mg I, Ca II, Zn II, Mg II, Fe II, and Cr II (see Paper II).

We compare the high ion profiles in Figure 5*a* (Si IV vs. C IV) and Figure 5*b* (C IV vs. N V). The individual error bars have been omitted in these comparisons but can be determined with reference to Figure 4. Ionic ratios are shown as a function of velocity in Figures 5*c* and 5*d*. In the velocity range from -70 to -40 km s^{-1} where there is very little Si IV, the C IV to N V column density ratio ranges from approximately 0.7 to 1.3. Over the velocity range from 0 to $+60$ km s^{-1}, the C IV and Si IV profile shapes are very similar with $N_a(v)_{\rm C\,IV}/N_a(v)_{\rm Si\,IV} = 3.5$.

4.2. *Equivalent Widths and Integrated Column Densities*

The equivalent widths, W_λ, of the high ion lines are listed in Table 3 along with the associated ± 1 σ uncertainty due to continuum placement and statistical uncertainties. We also list the values of the integrated column densities, log N_a,

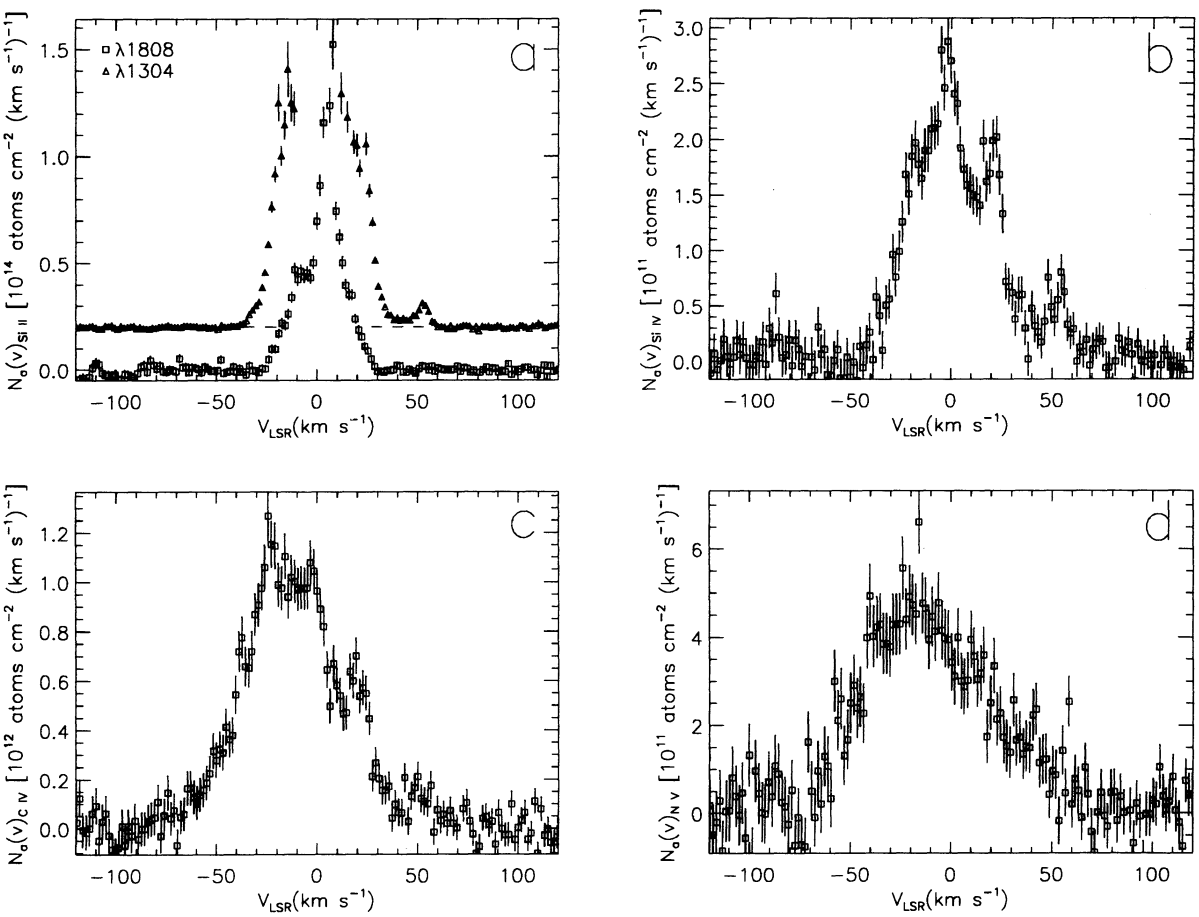

FIG. 4.—Apparent column density, $N_a(v)$ [atoms cm^{-2} (km s^{-1})$^{-1}$], vs. LSR velocity (km s^{-1}) for Si II, Si IV, C IV, and N V. The curves are based on the following absorption lines: Si II $\lambda\lambda$1808 and 1304, Si IV λ1393, C IV λ1548, and N V λ1238. The high ionization lines illustrated are fully resolved, and the values of $N_a(v)$ are a good representation of the actual $N(v)$. For Si II λ1808, the data near $+5$ km s^{-1} where the absorption is strongest are not plotted because the line has unresolved saturated structure. The Si II λ1304 curve provides information only about $N_a(v)$ at large negative and large positive velocities. The zero point from the curve for Si II λ1304 is offset by two tick marks and is plotted in the units [10^{13} atoms cm^{-2} (km s^{-1})] rather than [10^{14} atoms cm^{-2} (km s^{-1})$^{-1}$] which applies to the Si II λ1808 curve.

© American Astronomical Society • Provided by the NASA Astrophysics Data System

1994ApJ...420..183S

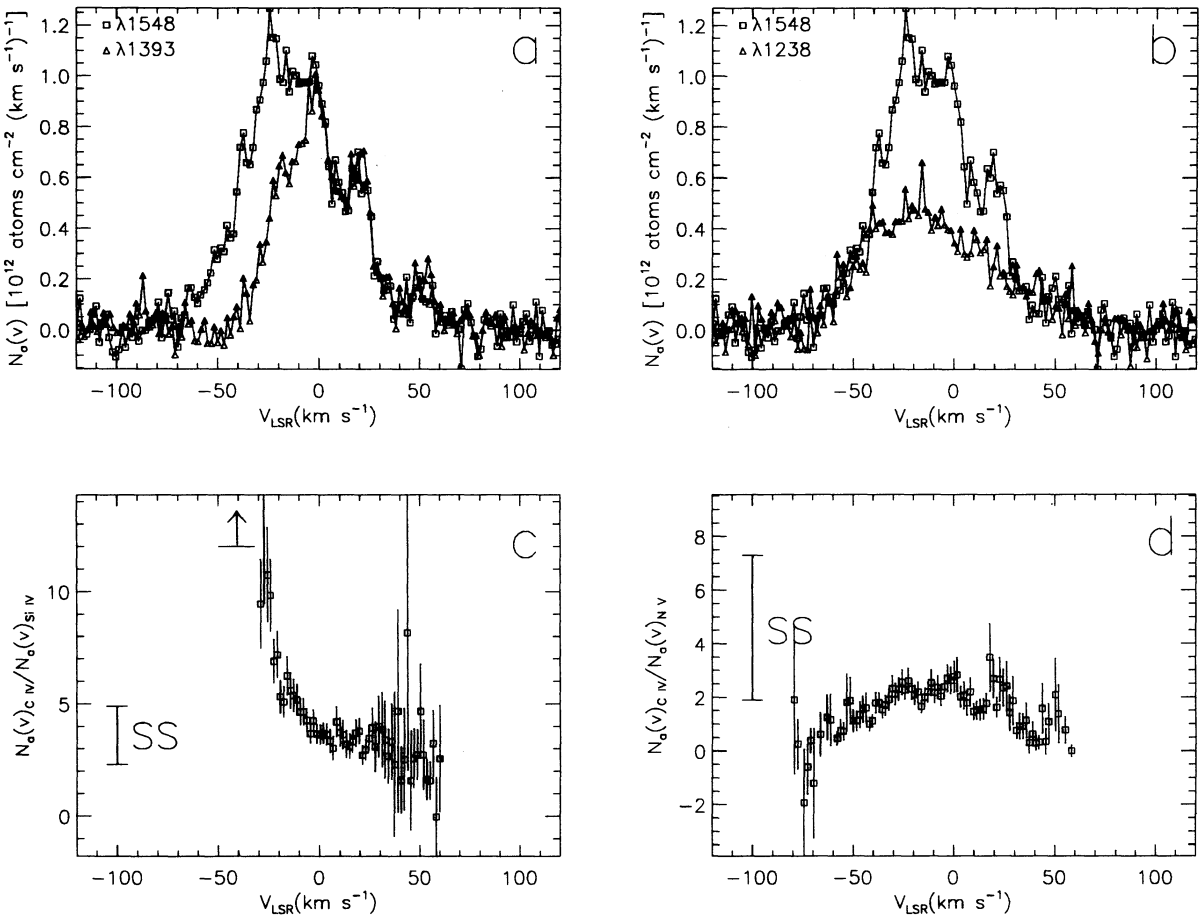

FIG. 5.—Curves of apparent column density, $N_a(v)$ [atoms cm^{-2} (km s^{-1})$^{-1}$], vs. LSR velocity (km s^{-1}) for Si IV, C IV, and N V are compared in the upper panels [(*a*) and (*b*)]. In the lower panels [(*c*) and (*d*)] ratios of apparent column density as a function of LSR velocity are shown. The $\pm 1\,\sigma$ range in these average ratios from Sembach & Savage (1992) are labeled SS in the lower two panels.

obtained by integrating the $N_a(v)$ profiles for each ion over the indicated velocity range. We average the values of log N_a listed in Table 4 to determine final logarithmic column densities of 13.09 ± 0.02, 13.83 ± 0.02, and 13.56 ± 0.03 for Si IV, C IV, and N V, respectively. The agreement in the values of log N_a for the two C IV lines indicates that unresolved saturation is not affecting the C IV data, and that the average of log N_a is equal to the actual integrated logarithmic column density, log N. A 1% background error, not included in the listed errors, will affect the column densities by approximately 0.005 dex. In determining these quantities, we have employed the continuum fitting and error calculation procedures used by Sembach & Savage (1992). The total column densities are in excellent agreement with the integrated values of log $N = 13.19 \pm 0.10$, 13.81 ± 0.06, and 13.60 ± 0.11 for Si IV, C IV, and N V based on an average of seven *IUE* spectra obtained at a resolution of 25 km s^{-1} (Sembach & Savage 1992). The excellent agreement illustrates that the *IUE* is capable of producing reliable integrated column densities for the high ion lines provided multiple spectra of high quality are averaged.

TABLE 3

HIGH ION EQUIVALENT WIDTHS AND INTEGRATED APPARENT COLUMN DENSITIES

Ion	λ (Å)	S/N[a]	$W_\lambda \pm 1\,\sigma$ (mÅ)	log N_a ($-1\,\sigma$)	log N_a Best	log N_a ($+1\,\sigma$)	Integration Range[b] v_- (km s^{-1})	Integration Range[b] v_+ (km s^{-1})
Si IV	1393.755	34	92.8 ± 3.6	13.07	13.09	13.11	−60	+75
C IV	1548.195	23	204.5 ± 5.6	13.81	13.82	13.84	−95	+75
	1550.774	32	121.0 ± 4.5	13.82	13.83	13.85	−95	+75
N V	1238.821	34	71.3 ± 3.5	13.54	13.56	13.59	−95	+75
	1242.804	38	37.0 ± 5.0	13.49:	13.56:	13.62:	−95	+75

[a] Approximate signal-to-noise ratio in the continuum at line center.
[b] Velocity integration range used in computing W_λ and N_a.

© American Astronomical Society • Provided by the NASA Astrophysics Data System

1994ApJ...420..183S

TABLE 4

HIGH ION COMPONENT STRUCTURE[a]

COMPONENT	$\langle v_i \rangle$ (km s^{-1})	b_i (km s^{-1})	log N_i			NOTES[b]
			$-1\,\sigma$	Best	$+1\,\sigma$	
Si IV ($\chi^2 = 1.01$)						
1	$+51.6 \pm 2.3$	12.0 ± 2.1	11.97	12.06	12.16	1
2	$+20.3 \pm 1.3$	10.0 ± 1.3	12.46	12.52	12.58	2
3	-0.5 ± 1.3	9.6 ± 1.5	12.56	12.64	12.71	3
4	-18.5 ± 2.9	11.6 ± 0.8	12.49	12.53	12.57	3
C IV ($\chi^2 = 1.04$)						
1	$+51.6 \pm 3.6$	12.3 ± 3.5	12.33	12.50	12.62	1
2	$+22.5 \pm 1.3$	9.9 ± 1.6	12.92	13.01	13.09	2
3	$+0.6 \pm 1.6$	10.4 ± 2.2	12.97	13.12	13.24	3
4	-19.7 ± 3.3	10.0 ± 1.9	12.80	12.93	13.03	3
5	-23.5 ± 7.8	26.8 ± 1.8	13.44	13.50	13.55	3
N V ($\chi^2 = 1.05$)						
1	$+25.2 \pm 10.6$	32.2 ± 8.7	12.82	12.98	13.13	3
2	-22.8 ± 3.9	32.6 ± 1.7	13.40	13.43	13.46	3

[a] The results of profile fitting to the GHRS high ion echelle mode observations are listed along with their $\pm 1\,\sigma$ errors. The various quantities listed for each component are central velocity, $\langle v_i \rangle$; Doppler spread velocity, b_i; and logarithmic column density.

[b] NOTES.—(1) Isolated component; (2) Component semi-isolated—may be blend of two or more components; (3) Component is not isolated—may be a blend of two or more components.

4.3. *Component Structure in the High Ion Absorption*

The high ion profiles are complex. The Si IV λ1393 and C IV λ1548 profiles have narrow components centered near -18, 0, $+21$, and $+52$ km s^{-1}. C IV also has a broad component near -23 km s^{-1}. The N V profiles are asymmetric and relatively featureless. However, the weakness of the N V absorption may make weak narrow features difficult to detect given the quality of the data. This detection problem is apparent when comparing the visibility of the narrow components in the C IV profiles for the weak and strong members of the doublet.

To obtain information about the properties of this structure and its relevance to the general absorption properties of the sight line, we fitted Gaussian components to the Si IV λ1393, C IV λ1548, and N V λ1238 profiles using the component-fitting procedure outlined by Sembach et al. (1993). In the fitting process, we accounted for the instrumental spread function by assuming it to be a Gaussian with FWHM = 3.5 km s^{-1}, and we used the smallest number of components possible to give a "good" ($\chi^2 \sim 1$) fit to the observed profiles. We fitted all three profiles independently of one another. We carried the errors on the individual data points through the minimization process to estimate a value of χ^2 and to calculate errors in the individual quantities describing each component: a central velocity, $\langle v_i \rangle$; a Doppler spread parameter, b_i; and a component column density, N_i.

The results of the profile fitting process are listed in Table 4 and are illustrated in Figure 6. We fit two, four, and five components to the N V, Si IV, and C IV profiles, respectively. These fits are by no means unique, but they are as valid as any other kinematical models given the low values of χ^2 (see Table 4) and our insufficient knowledge of the "true" component structure along the sight line. Of the components listed, only the $+52$ km s^{-1} component seen in Si IV and C IV is completely isolated from the main absorption. The component near $+21$ km s^{-1} seen in Si IV and C IV is located at the positive velocity edge of the main absorption in these two species and is partially isolated. The central velocities of Si IV and C IV components 1–4 are statistically identical and have very similar b values, whereas component 5 is seen in C IV but not in Si IV. This C IV component has a large b value ($+26.8$ km s^{-1}) and has a velocity similar to the velocity of component 2 found in N V.

To allow for other possible interpretations of the high ion absorption, we also fit the Si IV λ1393 profile with a large number of narrow components having widths ($b = 2.44$ km s^{-1}) appropriate for Si IV produced by photoionization in $T = 10^4$ K gas. Both the column densities and central velocities were allowed to vary for all components in the fit. A total of 16 photoionized components are required to match the quality of the fit given by the four Si IV components listed in Table 4. The components have column densities of 0.3–1.3 $\times$ 10^{12} cm^{-2} and are offset from each other at about 5 km s^{-1} intervals.

The physical processes operating in interstellar space that may produce the narrow and broad features discussed in this section are considered in the discussions of §§ 5.1 and 5.2.

5. DISCUSSION

Understanding the origin of the highly ionized gas in the Galactic disk and halo is fundamental to an ultimate understanding of the physical state and distribution of the many gas phases that fill interstellar space. The GHRS measurements. illustrated in Figures 1–6 provide a very high resolution view of the absorption produced by three important high ions and their relationships to the absorption produced by the cooler neutral gas traced by Ca II and Si II.

The Si IV, C IV, and N V profiles trace at least two distinct types of highly ionized gas along the sight line to HD 167756. One type of gas produces the broad N V profile. The other type

© American Astronomical Society • Provided by the NASA Astrophysics Data System

1994ApJ...420..183S

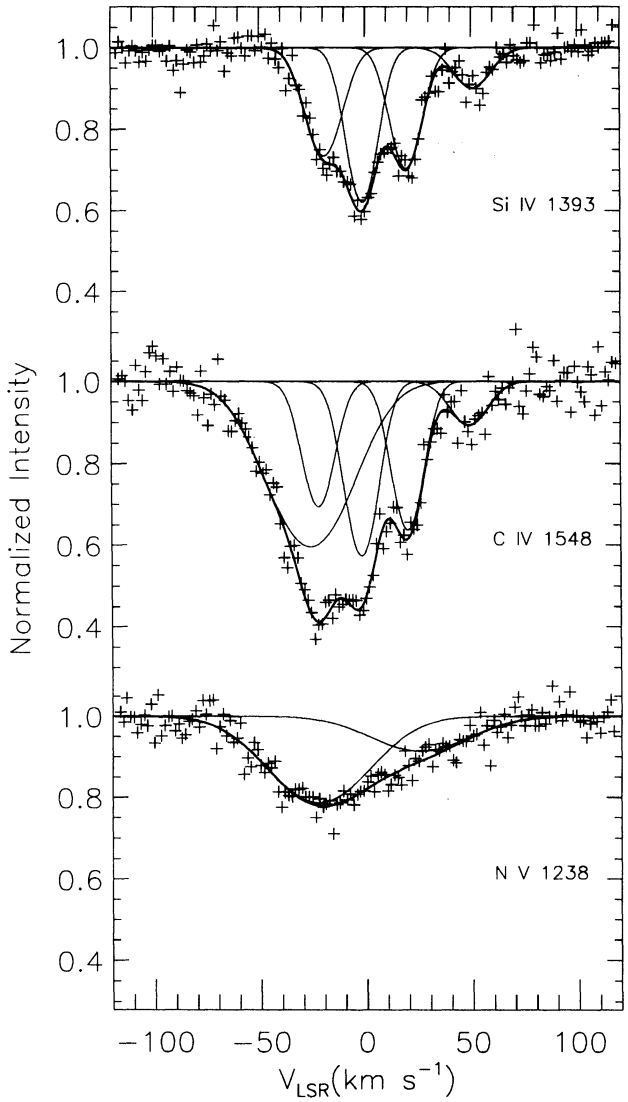

FIG. 6.—Gaussian profile fits to the absorption line data for Si IV λ1394, C IV λ1548, and N V λ1238. Normalized intensity is plotted against LSR velocity. The measurements are shown with plus signs. The lines show the results of the multicomponent fit described in § 4.3. For Si IV, C IV, and N V the fit process required four, five, and two components, respectively. The figure illustrates both the summed profiles (*heavily solid lines*) and the individual component profiles (*light solid lines*). The column densities, Doppler spread parameters, and velocities of the components are listed in Table 4.

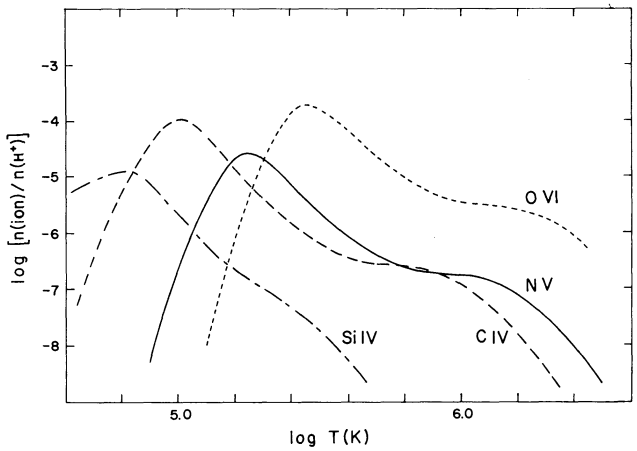

FIG. 7.—Curves of log [n(ion)/n(H$^+$)] vs. log T(K) for Si IV, C IV, N V, and O VI based on the equilibrium electron collisional ionization balanced by radiative and dielectronic recombination calculations of Sutherland & Dopita (1993). In the logarithmic system where [H] = 12.0, the adopted solar abundance values from Anders & Grevesse (1989) for C, N, O, and Si are 8.56, 8.05, 8.93, and 7.55, respectively.

produces the highly structured Si IV profile. The C IV profile contains contributions from both types of gas. We discuss each of these types of highly ionized gas in §§ 5.1 and 5.2.

5.1. *Smooth Broad* N V *Absorption: Evidence for Hot Gas*

Among the high ion lines accessible to the *HST*, N V is the best diagnostic of hot gas. N V is difficult to produce by photoionization because 77 eV is required for its creation, and the He^+ absorption edge in hot stellar atmospheres usually greatly reduces the emergent flux at energies above 54 eV. The relative abundances of Si IV, C IV, N V, and O VI in a hot plasma under conditions of collisional ionization equilibrium are illustrated in Figure 7 where we plot log [n(ion)/n(H$^+$)] versus log T(K). The figure was prepared using the solar abundances (Anders & Grevesse 1989) listed in the figure caption. The ionization equilibrium calculations are from Sutherland & Dopita (1993) and include the effects of dielectronic and radiative recombination and the most up to date atomic parameters. In the temperature range from log T = 4.6 to 6.0, these curves differ by <0.35 dex from the calculations of Arnaud & Rothenflug (1985). The secondary bumps on the higher temperature tails of these curves are caused by dielectronic recombination.

The broad, featureless, and asymmetric N V absorption profile extending from -70 to $+70$ km s^{-1} indicates the presence of hot gas along the sight line of HD 167756 (see Figs. 2 and 4*d*). The overall shape of the N V $N_a(v)$ profile is skewed to negative velocities by the modest amount of Galactic rotation toward HD 167756 (from 0 to -26 km s^{-1}). High-ionization absorption profiles toward inner Galaxy stars have previously been observed at modest resolution with the *IUE* satellite and have been modeled by Savage, Massa, & Sembach (1990) and Sembach, Savage, & Massa (1991). The model assumes a N V midplane density, n_0 (N V), an exponential scale height, H, and an intrinsic gas velocity dispersion modeled through an effective Doppler spread parameter, b. In this simple calculation the midplane density and the intrinsic velocity dispersion of the absorbing gas are assumed constant along the path to the star. For halo gas along the HD 167756 sight line, the additional assumption of corotation should be valid since the star is situated in the low halo at $z = -0.85$ kpc (Lockman 1984; Savage et al. 1990; Sembach et al. 1991). The best fit model curve of $N_a(v)$ for N V, shown in Figure 8, has n_0(N V) = 3.28 × 10^{-9} atoms cm^{-3}, H = 4 kpc, and b = 42 km s^{-1}. With such a simple model the data constrain only the velocity dispersion and midplane density and require the scale height to be large, $H > 2$ kpc. This scale height requirement fits well with the large scale heights found for the highly ionized ISM by Sembach & Savage (1992). The intrinsic velocity dispersion required to fit the N V profile, b = 42 km s^{-1}, is similar to values found previously by Savage et al. (1990) by Sembach et al. (1991) for other sight lines to inner Galaxy stars. Note that in these earlier papers the authors used a Gaussian dispersion, σ, rather than a Doppler spread parameter to allow for the effects of intrinsic kinematic and thermal broadening. The two quantities are related through $b = (2)^{1/2}\,\sigma$.

© American Astronomical Society • Provided by the NASA Astrophysics Data System

1994ApJ...420..183S

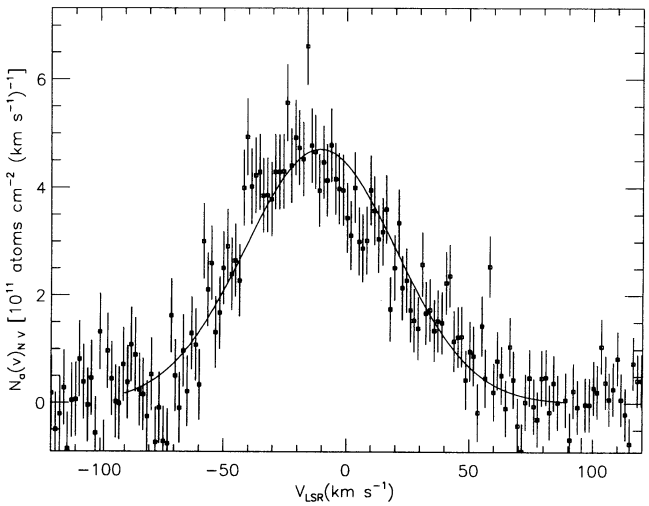

FIG. 8.—A model profile (*solid line*) is compared to the observed $N_a(v)$ profile for N V from Fig. 4*d*. The best-fit model profile is for an absorbing gas with a large exponential scale height ($H = 4$ kpc), a mid-plane density of n_0(N V) = 3.28×10^{-9} atoms cm^{-3}, and a combination of thermal and turbulent broadening that provides an effective Doppler broadening parameter, $b = 42$ km s^{-1}.

In the velocity range from −70 to −40 km s^{-1} significant N V and C IV absorption is seen while Si IV absorption is absent. At these velocities we can obtain information about the gas producing the broad N V absorption without the interfering confusion from absorption by the type of gas that produces the structured C IV and Si IV absorption between −40 and +30 km s^{-1}. In the range $v = -70$ to −40 km s^{-1}, the C IV to N V abundance ratio ranges from approximately 0.7 to 1.3 (Fig. 5*d*). This abundance ratio range is consistent with the component fits given in Table 4 for which it seems reasonable to associate the broad C IV component 5 ($\langle v \rangle = -23.5 \pm 7.8$ km s^{-1}; $b = 26.8 \pm 1.8$ km s^{-1}; log $N = 13.50 \pm 0.06$) with the broad N V component 2 ($\langle v \rangle = -22.8 \pm 3.9$ km s^{-1}; $b = 32.6 \pm 1.7$ km s^{-1}; log $N = 13.43 \pm 0.03$). From the two column densities we obtain a C IV to N V abundance ratio of 1.2 ± 0.25.

Referring to the equilibrium ionization calculations shown in Figure 7 we see that C IV to N V abundance ratios in the range from 0.7 to 1.3 occur near log $T = 5.2$ and 5.9 if the gas has a solar carbon to nitrogen abundance ratio. The absence of Si IV at $v < -40$ km s^{-1} is consistent with the negligible amounts for the ion expected at these temperatures. The two values of temperature are not strongly constrained. Deviations from the adopted solar C to N abundance ratio will shift the vertical positions of the curves for C IV and N V in Figure 7. The value of 3.23 we have adopted for the ratio of C to N (Anders & Grevesse 1989) is larger than that found for early-B stars (C/N = 2.57; Gies & Lambert 1992) and lies within the range of values recently reported for the Orion nebula (C/N = 2.45, Baldwin et al. 1991; C/N = 5.01, Rubin et al. 1991). The long (4 kpc) sight line to HD 167756 into the inner Galaxy may also begin to sample the effects of Galactocentric abundance gradients. The gradient for [N/H] of −0.12 dex kpc^{-1} is better determined than that for [C/H] of −0.09 dex kpc^{-1} (Peimbert 1992). If these gradients are correct, the differential gradient between C and N is only 0.03 dex kpc^{-1}, and we expect a 0.12 dex effect over the 4 kpc path to HD 167756. An overall uncertainty of about a factor of 1.5 in the C to N reference abundance ratio suggested by the abundances listed above will limit the significance of temperature constraints that can be inferred from observed C IV to N V column density ratios in some of the discussions which follow.

We first consider the possibility that the gas is at the lower temperature estimate of log $T = 5.2$. At this temperature the thermal Doppler contribution to the absorption line profiles would be described by a Doppler spread parameter $b = (2kT/m)^{1/2} = 14.8$ km s^{-1} for C IV and 13.7 km s^{-1} for N V. The N V profile fit discussed above and displayed in Figure 8 requires a Doppler spread parameter $b = 42$ km s^{-1}. Therefore, a temperature log $T = 5.2$ would require that the large width of the N V profile be due to a combination of thermal Doppler broadening and the broadening produced by a multiple-component absorbing medium with a turbulent velocity dispersion described by a Doppler parameter, b_{turb}, of ≈ 40 km s^{-1}.

If the gas is at log $T = 5.2$, it must have a small filling factor, f. This result follows from an estimate of its pressure:

$$P/k = 2.3 T n_0(\text{N V})[n(\text{H}^+)/n(\text{N V})] f^{-1} . \quad (3)$$

The factor of 2.3 allows for the number of particles including electrons provided by fully ionized hydrogen and helium. For $T = 1.6 \times 10^5$, n_0(N V) = 3.28×10^{-9} atoms cm^{-3}, and $[n(\text{H}^+)/n(\text{N V})] = 4 \times 10^4$ from Figure 7, we obtain $P/k = 48 f^{-1}$ atoms cm^{-3} K. To achieve reasonable interstellar medium thermal pressures (say $P/k \sim 5000$ particles cm^{-3}), the N V–bearing gas can occupy only a small fraction of the sight line, $f \sim 0.01$. Such a gas might occur in the conductive interface between a warm medium and a hotter medium. However, we do not believe this is a viable explanation for the gas absorbing in the velocity range from −70 to −40 km s^{-1}. Although a weak absorption component near −50 km s^{-1} is detected in the strong line of C II λ1334.532 and possibly Si III λ1206.500 (see Tripp, Sembach, & Savage 1993), the general velocity range from −70 to −40 km s^{-1} is relatively devoid of lower ionization gas required to provide the interfaces (see Ca II and Si II profiles in Figs. 1 and 2).

We next consider the possibility the gas producing the broad N V absorption and some of the C IV absorption is at the higher temperature log $T = 5.9$ suggested by the C IV to N V ratio in the velocity range from −70 to −40 km s^{-1}. In gas with log $T = 5.9$ the thermal Doppler parameter for N V is $b = 31$ km s^{-1}. Therefore, the observed Doppler parameter of 42 km s^{-1} inferred for N V could be interpreted as resulting from a combination of thermal broadening with $b \sim 31$ km s^{-1} and macroscopic turbulence with $b_{turb} \sim 28$ km s^{-1}. If the gas is near log $T = 5.9$, its pressure, from equation (3) with n_0(N V) = 3.28×10^{-9} atoms cm^{-3} and $[n(\text{H}^+)/n(\text{N V})] = 4 \times 10^6$ from Figure 7, is $P/k = 2.4 \times 10^4 f^{-1}$. With its interpretation, the hot gas must exist in a region with substantial pressure even if it fills much of the volume along the sight line. Such a high pressure may be reasonable for a sight line that passes through an active region of the Galaxy that contains candidate Galactic worms and supershells (see § 3).

If time-dependent processes are important, it is possible the actual pressure is lower. Gas with log $T = 5.0$–5.5 K cools so rapidly it is reasonable to question the assumption of ionization equilibrium in the preceding discussion. Since a cooling plasma will cool faster than it recombines (Shapiro & Moore 1976), the temperature of the cooling gas will be smaller than estimated from equilibrium models. Various time dependent theories have been advanced to explain the observed amounts

© American Astronomical Society • Provided by the NASA Astrophysics Data System

1994ApJ...420..183S

of highly ionized gas in the Galactic disk and halo. The observed broad N v absorption and the associated C iv absorption may be produced by the cooling gas of a Galactic fountain (Edgar & Chevalier 1986; Shapiro & Benjamin 1991, 1992) or by the superposition of a number of interfaces between hot (10^6 K) and warm (10^4 K) gas (Cowie & McKee 1977; Weaver et al. 1977; McKee & Ostriker 1978; Jenkins 1981; Borkowsky, Balbus, & Fristrom 1990). Spitzer (1990) provides an overview of the nature of the physical processes that might control the behavior of various types of evaporating envelopes between cold and hot media. The cooling remnants of supernova bubbles along the sight line (Slavin & Cox 1993) and the microflare heating model of Raymond (1992) also provide reasonable explanations for the high ion absorption. The above mentioned models yield C iv to N v ionic ratios in the range from 1.5 to 3.6 (see Table 10 of Sembach & Savage 1992). Some of the models have ratios close to the observed value which ranges from approximately 0.7 to 1.3 for velocities in the range from -70 to -40 km s^{-1}, but the interface models have the serious problem that the cooler gas is not detected at $v < -40$ km s^{-1}. The turbulent mixing layer model of Slavin, Shull, & Begelman (1993) produces to much C iv with C iv/N v predicted to be in the range from 10 to 30 depending on the model parameters.

Unfortunately, the number of models which can explain the data far exceeds the number of observational constraints now available. However, the very existence of the broad N v absorption and the associated C iv absorption rules out photoionized halo models that do not involve hot interstellar gas. A summary of the predictions of photoionized halo models is found in Sembach & Savage (1992). In all cases very little N v is produced.

The N v absorption may be revealing the effects of the venting of hot gas into the Galactic halo by a superposition of a number of Galactic shells and supershells along the sight line to HD 167756. The possibility that absorption by N v is providing a direct diagnostic of a phase of the interstellar medium with high temperature in regions of substantial Galactic interstellar activity is important for future studies of the interstellar medium with the *HST*.

5.2. *The Structured* Si iv *and* C iv *Absorption: Evidence for Warm-Hot Gas Interfaces*

In this section we consider the component structure common to both the Si iv and C iv profiles. The majority of this common velocity structure occurs over a range of positive velocities ($0 \leq v \leq 60$ km s^{-1}) "forbidden" by strict adherence of the gas to Galactic rotation. Given the apparent complexity of the profiles, there must be multiple absorbing regions along the sight line. It is not possible to directly assign a location to this positive velocity gas based upon its kinematic properties. Gas within spiral arms often shows large peculiar absorption velocities relative to corotating gas and may be the source of some of this absorption. Absorption at positive velocities demonstrates that some of the high ion gas along the sight line has peculiar motions with respect to the differential Galactic rotation law which predicts radial velocities from 0 to -26 km s^{-1}.

The C iv and Si iv profiles have strikingly similar shapes at positive velocities. This is clearly seen in Figure 5*a*, where we have plotted the column density per unit velocity for the two species as a function of LSR velocity. For $v > 0$ km s^{-1} we find $N_a(v)_{\rm C\ IV}/N_a(v)_{\rm Si\ IV} \approx 3.5$. The constancy of the ratio over this velocity range (see Fig. 5*c*) undoubtedly indicates a common origin for the two species at these velocities. The C iv to Si iv column density ratio of 3.5 throughout this range is the same as the integrated ratio found by Sembach & Savage (1992) for general sight lines through the Milky Way disk and halo, N(C iv)/N(Si iv) = 3.6 $\pm$ 1.3. The remarkable constancy of this ratio for sight lines into the Galactic halo was first recognized by Pettini & West (1982).

From a direct integration of the N v $N_a(v)$ profile from 0 to 60 km s^{-1}, we estimate that the amount of N v associated with the positive velocity Si iv and C iv is log N(N v) $\leq$ 13.10 (2 σ). If much of the N v arises in gas associated with the featureless N v absorption at negative velocities, we can further constrain this N v limit by assuming the associated N v absorption has a profile at positive velocities similar to the profile seen in Si iv and C iv. Therefore, by subtracting from the observed N v profile a profile having the shape of the Si iv and C iv profiles at positive velocity until statistically significant structure was introduced into the residual N v profile, we obtain the more rigorous N v upper limit of log N(N v) $\leq$ 12.66 (2 σ) for gas associated with the structured Si iv and C iv. Using a value of log N(C iv) = 13.22 yields N(C iv)/N(N v) $\geq$ 3.6 for $v > 0$ km s^{-1}, consistent with the integrated Galactic average N(C iv)/N(N v) = 4.6 $\pm$ 2.6 found by Sembach & Savage (1992).

Using the derived widths and ± 1 σ errors of the high ion positive velocity components in Table 4, we have plotted in Figure 9 the allowable two-dimensional relationships between $b_{\rm turb}$ and T that satisfy the observed Si iv and C iv widths for each component. If the highly ionized gas is in collisional equilibrium and has a solar composition, then the observed column density ratios, $2 < N$(C iv)/N(Si iv) < 4, for the three positive velocity components indicate that the gas has a temperature $T = (0.7\text{–}0.8) \times 10^5$ K (Sutherland & Dopita 1993). The measured widths of the high ion component at $+52$ km s^{-1} are consistent with an origin at these temperatures if the turbulent velocity of the gas is $6.0 < b_{\rm turb} \leq 10.5$ km s^{-1}, whereas the 0 km s^{-1} component must have a somewhat smaller turbulent velocity, $b_{\rm turb} \leq 7.0$ km s^{-1}. The 1 σ errors on the width of the component at $+21$ s^{-1} are consistent with this gas being created in a cooler gas with a turbulent velocity, $b_{\rm turb}$ = 7–10

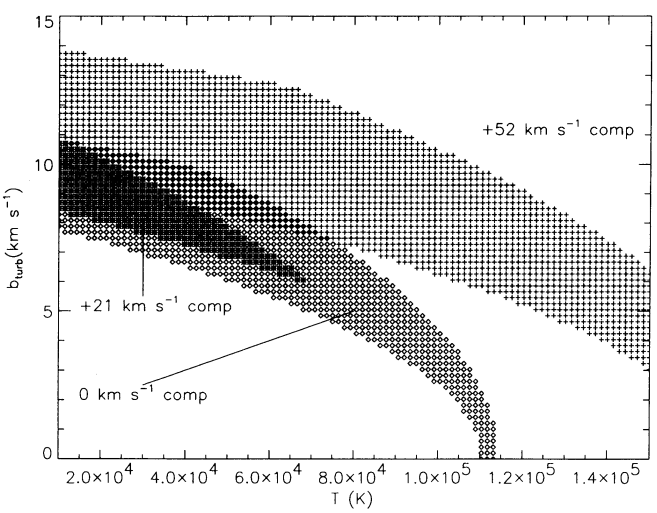

FIG. 9.—Allowed values of Doppler turbulent velocity, $b_{\rm turb}$, and temperature for the narrow components of Si iv and C iv detected near $v_{\rm LSR} = 0$, 21, and 52 km s^{-1} in the spectrum of HD 167756. Each shaded region is inferred from the values of b and their ± 1 σ errors listed in Table 4.

© American Astronomical Society • Provided by the NASA Astrophysics Data System

1994ApJ...420..183S

km s^{-1} for $T < 6.0 \times 10^4$ K. The gas creating the +21 km s^{-1} component cannot be in collisional equilibrium at a single temperature if both the observed Si IV and C IV column densities and widths must be simultaneously explained. In nonequilibrium situations, substantial fractions of the highly ionized gas may be present at lower temperatures (Shapiro & Moore 1976; Edgar & Chevalier 1986) which could be responsible for the observed quantities.

The similar overall extent of the Si IV λ1393 and Si II λ1304 profiles, $-40 \leq v \leq +60$ km s^{-1}, suggests that the neutral and the highly ionized gases producing the structured absorption are related. The high signal-to-noise ratio Ca II data from Sembach et al. (1993) reveals overlapping low ion components at LSR velocities of −36.2, −19.4, −11.3, −4.2, +6.5, +14.6, +22.7, and +51.6 km s^{-1}. The asterisk symbols below the Ca II profile in Figure 2 indicate the velocities of these components. Some of the structure within the Si IV and C IV profiles is correlated with low ion absorption structure. The correlation is most clearly seen in the +52 km s^{-1} component, where a range from low stages of ionization (C II*, O I, Si II, Fe II, Ca II) to high (Si IV, C IV) are seen. The high ion component at +21 km s^{-1} is not immediately identifiable in the Si II data shown in Figure 2, but is readily visible in the high signal-to-noise ratio Na I and Ca II data obtained by Sembach et al. (1993). Additional velocity component coincidences between the low and high ion lines occur to within a few km s^{-1} of each other, but the complexity of both the low- and high-ionization profiles prevents us from extracting detailed information about the gas relationships at those velocities. We consider the significance of the +21 and +52 km s^{-1} features for the origin of the highly ionized gas below but defer a more detailed discussion of the abundances and physical conditions in the neutral gas associated with these components to another paper (Tripp et al. 1993).

The observed Ca II Doppler parameters for the +22 and +52 km s^{-1} components are 7.3 ± 0.9 km s^{-1} and 3.7 ± 0.5 km s^{-1}, respectively. The turbulent velocities inferred from these widths are smaller than those we find for the high ion lines for gas temperatures $T < 6.5 \times 10^4$ K. Less than 1% of the observable calcium should be seen as Ca II for $T \geq 2.0 \times 10^4$ K in collisional equilibrium (Sutherland & Dopita 1993); therefore it is unlikely that the high and low ion gases are well mixed, even though they may share some common bulk motions.

The relationships between the neutral and highly ionized species in these two components suggest a set of interfaces occurring at neutral cloud boundaries. Two general possibilities for such interfaces are (1) low ion cloud boundaries photoionized by an external ionized field or (2) conduction fronts at low ion cloud boundaries evaporating or condensing in the presence of a hotter medium. We favor the second of these as the more likely source of the observed Si IV and C IV absorption at positive velocities.

To explain the observed Si IV profile as a group of photoionized components subject only to thermal broadening requires that at least 16 narrow absorption components, approximately twice the number of components observed in the high-resolution Na I and Ca II data for this sight line, be included in the model profile. Although the number of photoionized gas parcels necessary, one per 250 pc, does not conflict with the observed low ion absorption structure, it seems that such a simplistic picture of the high ion absorption is unlikely. If photoionization is occurring at the boundaries of clouds, there is likely to be some flowing motion of the gas as there is in H II regions around hot stars. H II regions typically have inferred turbulent velocities between 7 and 12 km s^{-1} (Reynolds 1991). These turbulent velocities often approach the local sound speed; at $T = 10^4$ K the speed of sound in a typical H II region is 10 km s^{-1} (Spitzer 1978; Osterbrock 1989). Thus, the widths of H II region components may be comparable to the observed widths of the Si IV and C IV components listed in Table 4 (see Fig. 9).

While the derived widths of the Si IV and C IV components are consistent with an H II region interpretation, the Si IV and C IV absorption observed toward HD 167756 cannot arise in classical H II regions around hot stars along the sight line (or in the HD 167756 H II region itself). Only one other known O or B star, HD 166596 (B2.5 III, d = 570 pc), is located within 1° of the sight line. The HD 167756 sight line passes within 10 pc of HD 166596, but this distance is still much larger than the predicted sizes of Si IV and C IV bearing regions around early-type stars (Cowie, Taylor, & York 1981). The observed C IV to Si IV ratio in H II regions is less than 1 for all but the hottest stars. For example, Sembach et al. (1993) find N(C IV)/N(Si IV) < 0.22 for the ζ Oph (O9.5 V) sight line, a ratio that is certainly larger than for H II regions that might be produced by either HD 166596 or HD 167756, and which is much smaller than the observed value of 3.5 found for the positive velocity gas toward HD 167756.

The most important reason for favoring a hot gas interface over the photoionized boundary interpretation of the positive velocity absorption is the constancy of the C IV to Si IV ratio at these velocities. Unless the ambient interstellar ionization field is remarkably uniform over the distances separating the gas parcels creating the positive velocity absorption, it is unclear why such a uniform ratio of these two ions should be produced given their different ionization potentials (48–65 eV for C IV vs. 33–45 eV for Si IV). The dominant sources of photons of these energies come from different sources within the Galaxy. O and B stars are the main source of photons with $E < 45$ eV, and the central stars of planetary nebulae are the prime source of photons with 45 eV < E < 54 eV (Bregman & Harrington 1986). The local ionization is also likely to vary from place to place with other factors such as gas density, cloud distribution, and abundance variations due to either elemental depletions or stellar activity.

The character of a planar interface between a cool or warm medium and a hot ($T > 5 \times 10^5$ K) medium in the presence of magnetic fields has been worked through in detail by Borkowski et al. (1990). Their work builds on earlier simplified dynamical investigations of hot gas interfaces (McKee & Cowie 1977; Weaver et al. 1977; Balbus & McKee 1982). The Borkowski et al. nonequilibrium ionization models make quantitative predictions of the velocity dispersions and column densities of the highly ionized gas as functions of magnetic field orientation, time, and initial conditions. One of the most important predictions of these models relatable to our observations is the relative constancy of the C IV to Si IV column density ratio for conduction fronts older than about $10^{4.5}$ yr, regardless of the magnetic field orientation relative to the front. Another important prediction is that thermal motions govern the line widths of the highly ionized species. The derived C IV components listed in Table 4 place the most stringent limits on the ages of the conduction fronts and indicate that the gas temperature must be $T < 1$–1.5×10^5 K. Temperatures in this range are appropriate for fronts in the late evaporative stage or

© American Astronomical Society • Provided by the NASA Astrophysics Data System

1994ApJ...420..183S

even early condensing stage when radiative losses are important, $t > 10^6$ yr (see Fig. 7 of Borkowski et al. 1990 for a plot of mean ionic temperature as a function of time). For similar reasons, a general preference for older fronts has been expressed by Borkowski et al. to explain the observed O VI profile widths reported for many stars (Jenkins & Meloy 1974; Jenkins 1978).

One might inquire whether the constancy of the column density ratios of species such as C IV, Si IV, and N V necessarily implies that the observed column densities themselves should also be constant. This is an important issue given that the observed column densities of C IV and Si IV vary by a factor of about 4 from 0 to $+52$ km s^{-1}. The column densities of Si IV and C IV are relatively insensitive to the initial temperature of the hot gas (for $T > 5 \times 10^5$ K) because of the relatively low ionization potentials of these species. However, the column densities may vary as a result of geometric projection effects or orientation of the magnetic field relative to the conduction front (see Borkowski et al. 1990). The number of fronts intercepted along the sight line at any particular velocity will also affect the column density of the species at that velocity.

The most glaring discrepancy between the observations and most of the hot gas models in the literature is that the models underestimate the amount of observable Si IV by a factor of 3–10. Allowing for silicon in dust increases the size of the discrepancy. This underestimate most likely results from the absence of incorporation of He II λ304 (and other lines) photons produced within the recombining gas. The strong λ304 line is capable of ionizing Si III but not C IV and N IV (see Sembach & Savage 1992 for a further discussion of this problem). The He II λ304 line becomes important in the late evaporative stages ($t > 3 \times 10^5$ yr) of the magnetized conduction front models discussed above. Other hot gas models that carry through the detailed radiative transfer calculations and incorporate the self-ionizing radiation effects on the ionization of the gas are capable of reproducing the observed high ion column density ratios (Shapiro & Benjamin 1991, 1992). Realistic models will also be needed to consider the effects of carbon and silicon depletion because of the possible existence of carbonaceous and silicate grains in the interface regions.

6. SUMMARY

The results of our high-resolution study with the GHRS of interstellar Si IV, C IV, and N V absorption in the spectrum of HD 167756 ($l = 351.^\circ5$, $b = -12.^\circ3$, $d = 4.0$ kpc, $z = -0.85$ kpc) are as follows:

1. The fully resolved high ion profiles have large extensions to negative and positive velocity. The Si IV profile extends from -40 to $+70$ km s^{-1} and has FWHM ≈ 52 km s^{-1}. C IV and N V extend from -70 to $+70$ km s^{-1} and have FWHM ≈ 67 and 73 km s^{-1}, respectively. The integrated logarithmic column densities for Si IV, C IV, and N V are 13.09 ± 0.02, 13.83 ± 0.02, and 13.56 ± 0.03, respectively.

2. The N V profile is broad and featureless, while the Si IV profile contains narrow absorption components centered near -19, 0, $+21$, and $+52$ km s^{-1} with Doppler spread parameters $b \sim 10$–12 km s^{-1}. The C IV profile contains broad and narrow structure.

3. The Si IV and C IV component near $+52$ km s^{-1} is associated with an intermediate-velocity feature detected in O I, Si II, Fe II, and Ca II. The other narrow high ion components all occur within several km s^{-1} of components also seen in low ionization gas

4. The high ion measurements indicate that the sight line contains at least two types of highly ionized gas. One type of gas is responsible for the broad smooth profile seen in the N V doublet lines. The other type of gas is responsible for the more structured profile found for the Si IV λ1393 line. The C IV doublet profiles contain contributions from both types of gas.

5. The broad asymmetric N V profile is well represented by an absorbing gas having a large scale height and a combination of turbulent and thermal broadening producing an effective Doppler spread parameter of 42 km s^{-1}. The N V absorption profile for this gas is influenced by a small amount of differential Galactic rotation (from 0 to -26 km s^{-1}) between the Sun and HD 167756. The C IV to N V abundance ratio of 1.0 ± 0.3 for this gas implies $T \sim 1.6 \times 10^5$ K or $\sim 8 \times 10^5$ K if the gas is in collisional ionization equilibrium and has a solar carbon to nitrogen abundance ratio. This absorption may be associated with cooling hot gas in Galactic shells and supershells along the sight line.

6. The high ion gas producing the structured Si IV absorption and part of the C IV absorption has a C IV to Si IV ratio of 3.5 over the velocity range from 0 to $+60$ km s^{-1}. The similarity of Si IV and C IV profile shapes indicates a common origin for the structured absorption seen in these two species. The correspondence in velocity extent and component structure of the Si II and Si IV lines indicates that the absorption by the neutral gas and the structured absorption by the highly ionized gas is related. The process producing the structured Si IV and C IV absorption evidently has a regulation mechanism that favors a C IV to Si IV ionic ratio of 3.5. We believe this absorption is most likely due to conductive interfaces along the sight line.

We thank the many people involved with the *HST* and GHRS programs for making the observations reported in this paper possible. We have received helpful comments on various aspects of the research contained in this paper from D. Cox, R. Edgar, J. Mathis, J. Raymond, R. Reynolds, L. Spitzer Jr., U. J. Sofia, J. M. Shull, and T. Tripp. We thank D. Massa for providing the software used to model the N V profile. B. D. S. acknowledges support for this research through NASA grant NAG 5-1852. K. R. S. appreciates support as a Hubble Fellow though grant HF-1038.101-92A from the Space Telescope Science Institute, which is operated by AURA under NASA contract NAS 5-26555. J. A. C. acknowledges support from NASA grant NAGW-2520.

REFERENCES

Anders, E., & Grevesse, N. 1989, Geochim. Cosmochim. Acta, 53, 197
Arnaud, M., & Rothenflug, R. 1985, A&AS, 60, 425
Balbus, S. A., & McKee, C. F. 1982, ApJ, 252, 529
Baldwin, J. A., Ferland, G. M., Martin, P. G., Corbin, M. R., Cota, S. A., Peterson, B. M., & Settlebak, A. 1991, ApJ, 374, 433
Borkowski, K. J., Balbus, S. A., & Fristrom, C. C. 1990, ApJ, 355, 501
Bregman, J. N., & Harrington, J. P. 1986, ApJ, 309, 833
Cardelli, J. A., Ebbets, D. C., & Savage, B. D. 1990, ApJ, 365, 789
Cardelli, J. A., Ebbets, D. C., & Savage, B. D. 1993, ApJ, 413, 401
Cardelli, J. A., Savage, B. D., Bruhweiler, F. C., Smith, A. M., Ebbets, D. C., Sembach, K. R., & Sofia, U. J. 1991, ApJ, 377, L57
Cardelli, J. A., Sembach, K. S., & Savage, B. D. 1993, in preparation (Paper II)
Clemens, D. P. 1985, ApJ, 295, 422
Courtès, G., Georgelin, Y. P., & Monnet, G. 1970, in IAU Symp. 38, The Spiral Structure of Our Galaxy, ed. W. Becker & G. Cantopoulos (Dordrecht: Reidel), 209

© American Astronomical Society • Provided by the NASA Astrophysics Data System

1994ApJ...420..183S

Cowie, L. L., & McKee, C. F. 1977, ApJ, 211, 135
Cowie, L. L., Taylor, W., & York, D. G. 1981, ApJ, 248, 528
Danly, L., Lockman, F. J., Meade, M. R., & Savage, B. D. 1992, ApJS, 81, 125
Diplas, A., & Savage, B. D. 1993, ApJ, submitted
Duncan, D. K., & Ebbets, D. C. 1989, Goddard High-Resolution Spectrograph Instrument Handbook, Space Telescope Science Institute
Ebbets, D. 1992, Final Report of the Science Verification Program for the Goddard High Resolution Spectrograph for the *Hubble Space Telescope* (Boulder: Ball Aerospace Corp.)
Edgar, R. J., & Chevalier, R. A. 1986, ApJ, 310, L27
Garrison, R. F., Hiltner, W. A., & Schild, R. E. 1969, ApJ, 157, 313
———. 1977, ApJS, 35, 111
Georgelin, Y. P., & Georgelin, Y. M. 1976, A&A, 49, 57
Gies, D. R., & Lambert, D. L. 1992, ApJ, 387, 673
Jenkins, E. B. 1978, ApJ, 220, 107
———. 1981, in The Universe at Ultraviolet Wavelengths, ed. R. D. Chapman (NASA CP-2171), 541
Jenkins, E. B., & Meloy, D. A. 1974, ApJ, 193, L121
Johnson, H. L. 1963, in Stars and Stellar Systems, 3, Basic Astronomical Data, ed. K. A. Strand (Chicago: Univ. of Chicago Press), 214
Joseph, C. L., & Jenkins, E. B. 1991, ApJ, 368, 201
Koo, B.-C., Heiles, C., & Reach, W. T. 1992, ApJ, 390, 108
Lockman, F. J. 1984, ApJ, 283, 90
McKee, C. F., & Cowie, L. L. 1977, ApJ, 215, 213
McKee, C. F., & Ostriker, J. P. 1978, ApJ, 218, 148
Mihalas, D., & Binney, J. 1981, Galactic Astronomy (2d ed.; New York: W. H. Freeman)
Moore, C. E. 1970, Ionization Potentials and Ionization Limits Derived from the Analysis of Optical Spectra (NSRDS-NBS Rep. 34) (Washington, DC: US Dept. of Commerce)
Morton, D. C. 1991, ApJS, 77, 119
Oort, J. H. 1970, ARA&A, 15, 295
Osterbrock, D. E. 1989, Astrophysics of Gaseous Nebulae and Active Galactic Nuclei (Mill Valley: University Science Books), chap. 6
Peimbert, M. 1992, in The Astronomy and Astrophysics Encyclopedia, ed. S. P. Maran (New York: van Nostrand Reinhold), 356
Pettini, M., & West, K. A. 1982, ApJ, 260, 561
Raymond, J. 1992, ApJ, 384, 502
Rickard, J. J. 1974, A&A, 31, 47
Rubin, R. H., Simpson, J. P., Hass, M. R., & Erickson, E. F. 1991, ApJ, 374, 564
Savage, B. D., Cardelli, J. A., & Sofia, U. J. 1992, ApJ, 401, 706
Savage, B. D., & Massa, D. 1987, ApJ, 314, 380
Savage, B. D., Massa, D., & Sembach, K. S. 1990, ApJ, 355, 114
Savage, B. D., & Sembach, K. R. 1991, ApJ, 379, 245
Schild, R. E., Garrison, R. F., & Hiltner, W. A. 1983, ApJS, 51, 321
Sembach, K. R., Danks, A., & Savage, B. D. 1993, A&AS, 100, 107
Sembach, K. R., & Savage, B. D. 1992, ApJS, 83, 147
Sembach, K. R., Savage, B. D., & Jenkins, E. B. 1994, ApJ, in press
Sembach, K. R., Savage, B. D., & Massa, D. 1991, ApJ, 372, 81
Shapiro, P. R., & Benjamin, R. A. 1991, PASP, 103, 923
———. 1992, in Star Forming Galaxies and Their Interstellar Media, ed. J. J. Franco (New York: Cambridge Univ. Press), in press
Shapiro, P. R., & Moore, R. T. 1976, ApJ, 207, 460
Slavin, J. D., & Cox, D. P. 1993, ApJ, in press
Slavin, J. D., Shull, J. M., & Begelman, M. C. 1993, ApJ, 407, 83
Spitzer, L., Jr. 1978, Physical Processes in the Interstellar Medium (New York: Wiley & Sons), chap. 11
———. 1990, ARA&A, 28, 71
Spitzer, L., & Fitzpatrick, E. L. 1992, ApJ, 391, L41
Sutherland, R. S., & Dopita, M. A. 1993, ApJS, 88, 253
Tripp, T. M., Sembach, K. R., & Savage, B. D. 1993, in preparation
Walborn, N. R. 1972, AJ, 77, 312
Weaver, R., McCray, R., Castor, J., Shapiro, P., & Moore, R. 1977, ApJ, 218, 377
Wilson, R. E. 1953, General Catalog of Stellar Radial Velocities (Carnegie Inst. of Washington Pub. 601) (Washington: Carnegie Institute of Washington)

© American Astronomical Society • Provided by the NASA Astrophysics Data System